On 1:3 resonance under reversible perturbations of conservative cubic Hénon maps

M. S. Gonchenko[1], A. O. Kazakov[2], E. A. Samylina[2,3], A. I. Shykhmamedov[2]

[1] Universitat Politècnica de Catalunya, Barcelona, Spain

[2] National Research University Higher School of Economics, Nizhny Novgorod, Russia

[3] Lobachevsky State University of Nizhny Novgorod, Nizhny Novgorod, Russia

marina.gonchenko@upc.edu, kazakovdz@yandex.ru, samylina_evgeniya@mail.ru, aykhansh@gmail.com

May 5, 2021

Abstract

We consider reversible non-conservative perturbations of the conservative cubic Hénon maps $H_3^{\pm} : \bar{x} = y, \bar{y} = -x + M_1 + M_2 y \pm y^3$ and study their influence on the 1:3 resonance, i.e. bifurcations of fixed points with eigenvalues $e^{\pm i2\pi/3}$. It follows from [DM00], this resonance is degenerate for $M_1 = 0, M_2 = -1$ when the corresponding fixed point is elliptic. We show that bifurcations of this point under reversible perturbations give rise to four 3-periodic orbits, two of them are symmetric and conservative (saddles in the case of map H_3^+ and elliptic orbits in the case of map H_3^-), the other two orbits are nonsymmetric and they compose symmetric couples of dissipative orbits (attracting and repelling orbits in the case of map H_3^+ and saddles with the Jacobians less than 1 and greater than 1 in the case of map H_3^-). We show that these local symmetry-breaking bifurcations can lead to mixed dynamics due to accompanying global reversible bifurcations of symmetric non-transversal homo- and heteroclinic cycles. We also generalize the results of [DM00] to the case of the $p : q$ resonances with odd q and show that all of them are also degenerate for the maps $H_3^{\pm}$ with $M_1 = 0$.

1 Introduction

In the present paper we study how reversible non-conservative perturbations affect the 1:3 resonance, i.e. bifurcations of fixed points with eigenvalues $e^{\pm i2\pi/3} = -1/2 \pm i\sqrt{3}/2$, in the conservative cubic Hénon maps

$$H_3^{\pm} : (x, y) \to (\bar{x}, \bar{y}) : \bar{x} = y, \quad \bar{y} = -x + M_1 + M_2 y \pm y^3, \qquad (1)$$

where x and y are coordinates, M_1 and M_2 are real coefficients. This problem is of great interest since it is closely related to the so-called phenomenon of mixed dynamics [Gon16, GT17, GGK20], the third recently discovered type of chaos (in addition to the well-known conservative and dissipative chaos) which is characterized by the principal inseparability of conservative and dissipative elements of dynamics. Indeed, the cubic Hénon maps (1) appear as truncated first return maps near cubic homoclinic tangencies in area-preserving diffeomorphisms [GGO17]. Note that the different signs ± 1 before the cubic term y^3 correspond to two different types of cubic homoclinic tangencies, see [Gon85, GSV13, GGO17] for more details. In the case of reversible maps, the appearance of such symmetric

1

homoclinic tangencies is a codimension 1 bifurcation phenomenon [GGS20]. On the other hand, the existence of homoclinic tangencies implies the existence of Newhouse domains where such tangencies, including symmetric cubic homoclinic tangencies in the reversible case, are dense [GGS20]. In turn, the emergence of symmetric pairs of nonsymmetric orbits provides a criterion of the appearance of mixed dynamics. Namely, in these Newhouse domains, maps with infinitely many periodic sinks (also called stable or attracting orbits), sources (completely unstable or repelling orbits), area-expanding saddles (with the Jacobian greater than 1) and area-contracting saddles (with the Jacobian less than 1) as well as symmetric elliptic periodic orbits are dense.

It is widely known that the strong 1:1, 1:2, 1:3 and 1:4 resonances, i.e. bifurcations of fixed points (periodic orbits) with eigenvalues $e^{\pm 2\pi i/q}$, $q = 1, 2, 3, 4$, respectively, are very important for dynamics. In the conservative setting, the nondegenerate 1:1 resonance is related to a parabolic (elliptic-hyperbolic) bifurcation of fixed (periodic) points that implies the appearance of a pair of saddle and elliptic orbits. In turn, the nondegenerate 1:2 resonance is connected with a conservative period-doubling bifurcation. The 1:3 and 1:4 resonances are most difficult, their theory was outlined in [Arn88], where, in particular, a case of the degenerate 1:4 resonance (the so-called "Arnold degeneracy") was considered, see also [AKN06]. A new, second, type of degenerate conservative 1:4 resonance has been found recently in [GGO17, GGOV18]. As well-known, the complex local normal form of an area-preserving map near a fixed point with eigenvalues $\pm i$ (1:4 resonance) is written as $\bar{z} = i(z + A|z|^2 z + B(z^*)^3) + O(|z|^5)$, where A and B are real coefficients. The Arnold degeneracy corresponds to the case $|A| = |B|$, the other degeneracy from [GGO17] is related to the case $B = 0$. The latter degeneracy is very interesting since it is accompanied by symmetry-breaking (pitchfork) bifurcations of 4-periodic orbits. Note that a class of degenerate $p : q$ resonances accompanied by symmetry-breaking bifurcations of q-periodic points was described in [GLRT14]. The 1:4 resonance fits well into this class [GGO17], while the 1:3 resonance has certain peculiarities. In particular, when the map possesses the central symmetry, four 3-periodic orbits appear near the 1:3 resonant fixed point: two of them are elliptic while the other two are saddle. In the present paper we also show that all $p : q$ resonances with odd $q \geq 3$ are degenerate for the cubic Hénon maps with the central symmetry (when $M_1 = 0$).

The strong resonances often appear in area-preserving maps. For example, in the conservative quadratic Hénon map $\bar{x} = y, \bar{y} = M - x - y^2$ the structure of the 1:4 resonance was studied in [Bir87], where it was shown that this resonance is degenerate (the Arnold case). In [Bir87] it was also shown that in the quadratic Hénon map, the 1:3 resonance is nondegenerate, and it mainly consists of the rearrangement of symmetric 3-periodic saddle orbits. Bifurcations in two-parameter families of area-preserving Hénon-like maps were also studied in [SV09]. In particular, in [SV09] it was demonstrated that the emergence of fixed point with eigenvalues $e^{\pm i2\pi/3}$ in the conservative quadratic Hénon map implies both local instability of the fixed point and global instability of the map, i.e the fixed point becomes saddle with 6 separatrices (local effect) and almost all orbits close to the fixed point go to infinity (global effect). However, this is not the case when the 1:3 resonance is degenerate. Here, in general, the fixed point is surrounded by a garland (a chain of stability islands) which consists of elliptic and saddle 3-periodic orbits and does not allow orbits to pass far away from the fixed point. This local stability also implies global stability when the 1:3 resonance is near-degenerate. Note that such a situation takes place in the conservative cubic Hénon maps (1), see Figures 3 and 4. Here a degenerate 1:3 resonance appears at $M_1 = 0$ and $M_2 = -1$, otherwise it is nondegenerate if $M_1 \neq 0$. We also note that all $p : q$ resonances with odd q have the same nature: they are degenerate for $M_1 = 0$ and the corresponding value of M_2, see Figure 5 for the 1:5 and 1:7 resonances.

Our main goal is to study the near-degenerate 1:3 resonance in (1) and analyze how it is impacted by reversible non-conservative perturbations. It follows from [DM00] that for $M_1 = 0$ and $M_2 = -1$,

the 1 : 3 resonance is degenerate for the conservative cubic Hénon maps and 3-periodic orbits undergo pitchfork bifurcations. We note that both maps H_3^+ and H_3^- are conservative and reversible with respect to the involution $h : (x, y) \to (y, x)$, i.e. by definition the maps $H_3^\pm$ and the inverse maps $(H_3^\pm)^{-1}$ are conjugate by means of the involution h (the relation $(H_3^\pm)^{-1} = h \circ H_3^\pm \circ h$ holds). In the general case, reversible maps can also have dissipative orbits that always exist in pairs: stable and completely unstable periodic orbits, two saddle periodic orbits with the Jacobian greater than 1 and less than 1, etc. Such orbits are symmetric to each other with respect to the involution. We call them a *symmetric couple of orbits*. When a map is reversible and conservative, symmetric couples of orbits are conservative, however, under general reversible perturbations, these pairs can become dissipative.

The genericity of perturbations means that they should destroy the conservativity. Following the paper [GGS21], we construct (analytically) such reversibility preserving perturbations. We present two direct methods to obtain such perturbations for the conservative cubic Hénon maps (1). The first method gives reversible non-conservative perturbations in the so-called cross-form (2), and, in this way, we obtain perturbations of the second iteration of the inverse cubic maps $(H_3^\pm)^{-2}$ in the form (5). The second method provides a perturbation of the cubic maps themselves, see the map (9). We illustrate the bifurcation diagrams for the near-degenerate 1:3 resonance in the perturbed maps and focus on pitchfork bifurcations of 3-periodic orbits which lead to the dissipative dynamics. Namely, we demonstrate that for perturbations of H_3^+ a supercritical pitchfork bifurcation takes place which leads to the emergence of nonsymmetric attracting and repelling 3-periodic orbits, while for perturbed map H_3^- under a subcritical pitchfork bifurcation there appears a pair of nonsymmetric saddles, one is with the Jacobian greater than 1 and the other is with the Jacobian less than 1.

The fact that mixed dynamics can often appear in applications was shown in [GGK13, GGKT17]. Recently, the number of the related results has sharply increased, see e.g. [Kuz17, Kuz18, EN19, Kaz19, AS20, EN20, BM20a, GGK20, BM20b, EN21]. In all these studies, two sides of the phenomenon of mixed dynamics come to light: first, to find it numerically or experimentally, i.e. to provide evidence that attractors and repellers intersect, and, second, to prove it mathematically. As far as we know, only in a couple of papers, see e.g. [GGKT17, Kaz20], both sides were analyzed. The second side (to prove) is much delicate than the first one, it requires involving various theoretical aspects of mixed dynamics such as criteria for the existence of absolute Newhouse regions [GST97, LS04, Tur10, GGS20] and the structure of bifurcation scenarios leading to the appearance of mixed dynamics, see e.g. [GGKT17, Kaz19, Kaz20]. In the present paper we apply both these approaches when studying local and global bifurcations.

The paper is organized as follows. In Section 2 we present the main elements of the theory of reversible systems, mixed dynamics and the associated symmetry-breaking bifurcations that we will use throughout the paper. In Section 3 we discuss the two methods to construct reversible non-conservative perturbations of the conservative Hénon-like maps and prove that the perturbed maps are indeed reversible. In this way, we obtain perturbations of the conservative cubic Hénon maps (1). In Section 4 we review the structure of bifurcations of the conservative 1:3 resonance and mention the associated degeneracies and pitchfork bifurcations of 3-periodic orbits for the unperturbed cubic maps $H_3^\pm$ in the form (5). Also in this section we show that all $p : q$ resonances with odd q are triple degenerate in maps $H_3^\pm$ with $M_1 = 0$. In Sections 6 and 7 we analyze reversible and nonconservative perturbations of H_3^+ and H_3^-, respectively, as well as display bifurcation diagrams for near-degenerate 1:3 resonance and demonstrate the appearance of dissipative 3-periodic orbits under pitchfork bifurcations in both cases. In Section 8 we provide numerical evidence of mixed dynamics in a reversible non-conservative perturbation of H_3^- and discuss possible emergence of mixed dynamics in the map H_3^+.

2 Reversible systems, mixed dynamics and symmetry-breaking bifurcations

In [GT17], it was established that multidimensional systems with the compact phase space can have three different and independent forms of dynamics. Two of them have been well known for a long time: these are *conservative* and *dissipative* dynamics, the third form, the so-called *mixed dynamics*, is rather new.

The most famous example of conservative dynamics is provided by systems which preserve phase volume (e. g. Hamiltonian systems, area- and volume-preserving maps). From the point of view of topological dynamics, the conservative dynamics is characterized by the fact that the phase space is chain-transitive [AB85, GT17], i.e. any two points can be connected by ε-orbits for any $\varepsilon > 0$. The dissipative dynamics has a completely different nature: the phase space is not chain-transitive and, besides, one can construct a set of nonintersecting absorbing and repelling domains containing, respectively, all attractors and repellers of the system.

As for the mixed dynamics, first of all, it is characterized by the principal inseparability of attractors and repellers [GST97], which implies the existence of infinitely many dissipative attractors and repellers and the impossibility of constructing a set of disjoint absorbing and repelling domains, see more details in [GT17, GGK20].

As well-known [Con78], any homeomorphism of a compact phase space has attractors and repellers. An attractor is considered in the Ruelle sense [Rue81] as a closed invariant and chain-transitive set which is stable under permanently acting perturbations[1], and a repeller is an attractor of the inverse map. In [GT17] it was shown that such attractors and repellers can have a non-empty intersection, in contrast to attractors and repellers that are attracting and repelling sets, i.e. asymptotically stable invariant sets under forward and backward iterations, respectively. Denote the full sets of such attractors and repellers of the phase space as $\mathcal{A}$ and $\mathcal{R}$, respectively. Such closed invariant sets are called *the full attractor* and *full repeller* of a map in [GT17]. Then the above classification of dynamics can be built according to the following principle [GT17]: if $\mathcal{A} = \mathcal{R}$, then the system demonstrates (topologically) conservative dynamics (in this case, $\mathcal{A}$ and $\mathcal{R}$ coincide with the whole phase space); if $\mathcal{A} \cap \mathcal{R} = \emptyset$, then the dynamics is dissipative; and $\mathcal{A} \cap \mathcal{R} \neq \emptyset$ and $\mathcal{A} \neq \mathcal{R}$ in the case of mixed dynamics. These logical relations constitute the complete system, and, therefore, there is no other type of dynamics demonstrated by homeomorphisms of compact phase spaces.

However, for concrete systems with chaotic dynamics, it is practically never known precisely what $\mathcal{A}$ and $\mathcal{R}$ are. Therefore, certain, efficiently verifiable criteria are needed to determine the type of dynamics. If such criteria are well known for conservative and dissipative dynamics, then, in the case of mixed dynamics, the situation is more complicated: all known criteria are quite nontrivial and are related to the existence of the so-called absolute Newhouse regions [GST97, Tur10, Tur15].

In the case of two-dimensional diffeomorphisms, there are such regions where diffeomorphisms with the following properties are generic[2]: (i) every such diffeomorphism has infinitely many periodic sinks, sources, and saddles and (ii) the closures of the sets of orbits of different types have non-empty intersections. In [GST97], it was proven that the absolute Newhouse regions exist in any neighborhood of a diffeomorphism with a non-transversal heteroclinic cycle that contains two saddle fixed points O_1 and O_2 and two heteroclinic orbits Γ_{12} and Γ_{21} such that $W^s(O_1)$ and $W^u(O_2)$ intersect at the points of Γ_{12} transversally, and $W^s(O_2)$ and $W^u(O_1)$ have a quadratic tangency at

---

[1]This type of stability is also called total stability or Lyapunov stability for ε-orbits and has been known for a very long time, see e.g. [Mal44]. In fact, this means the stability under arbitrary small bounded noise.

[2]The Newhouse regions are open in C^r-topology with $r \geq 2$, and a certain property is called generic if it holds for a residual subset (a set of the second Baire category) of diffeomorphisms of such region.
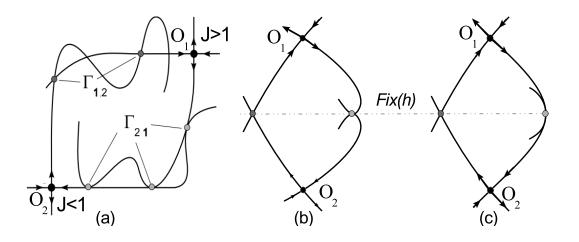
Figure 1: Examples of non-transversal heteroclinic cycles of planar diffeomorphisms: (a) the heteroclinic cycle studied in [GST97]; (b) the non-transversal heteroclinic cycle with a quadratic tangency from [LS04]; (c) the non-transversal heteroclinic cycle with a cubic tangency from [GGS20].

the points of Γ_{21}, see Figure 1a. The principally important condition is that the Jacobian of the map is greater than 1 at one of the fixed points and less than 1 at the other. This result shows that the mixed dynamics is a generic property of two-dimensional diffeomorphisms from absolute Newhouse regions: indeed, the sets $\mathcal{A}$ and $\mathcal{R}$ are closed invariant sets that should contain all sinks and sources, respectively, and, hence, the set $\mathcal{A} \cap \mathcal{R}$ is non-empty due to the above property (ii).

In the present paper we consider two-dimensional reversible diffeomorphisms. Recall that a diffeomorphism f is reversible if it is conjugate to its inverse map f^{-1} by means of an involution h, i.e. the following relation is true: $f^{-1} = h \circ f \circ h$, where $h^2 = Id$. The property of reversibility of f implies the strong symmetry of the set of orbits. An orbit that intersects the set $Fix(R) = \{x : R(x) = x\}$ or the set $Fix(Rf)$ is called *symmetric*. Any symmetric periodic orbit of a two-dimensional reversible orientable map has eigenvalues λ and λ^{-1}. Moreover, such an orbit with eigenvalues $e^{\pm i\varphi}$, where $\varphi \neq 0, \pi$, is, essentially, elliptic, since the principal hypotheses of the KAM theory hold [Sev86]. However, there are principal differences in dynamics. In particular, it was shown in [GLRT14, GT17] that a generic elliptic point of two-dimensional reversible maps is not completely conservative since it is the limit of periodic sinks and sources.

As for nonsymmetric orbits, they can be, in principle, of arbitrary type. However, for any nonsymmetric orbit, there exists a symmetric to it orbit with "opposite" dynamical properties. It means that if a periodic orbit has eigenvalues λ_1 and λ_2, then the symmetric to it orbit has eigenvalues λ_1^{-1} and λ_2^{-1}. As we said before, nonsymmetric orbits compose a symmetric pair of orbits.

As in the dissipative case, in the space of reversible systems, Newhouse regions (i.e. such open regions in which reversible systems with both symmetric and nonsymmetric homoclinic tangencies are dense) exist near any system with a symmetric homoclinic tangency. However, there is one non-trivial moment related to the proof of the fact that these regions are absolute Newhouse regions, i.e. that they contain a residual subset of systems having infinitely many coexisting periodic attractors, repellers, saddles and elliptic orbits and the closure of the sets of the orbits of different types has a non-empty intersection.

This problem, proposed in [DGGLS13] as the Reversible Mixed Dynamics conjecture (RMD-conjecture), remains open for the multidimensional case. For two-dimensional reversible maps, it was proved in [GLRT14] for C^r-perturbations (with $2 \leq r \leq \infty$) that keep the reversibility. Also

the RMD-conjecture was proved in [LS04, DGGLS13, DGGL18, GGS20] for some cases of one-parameter families unfolding generally symmetric couples of heteroclinic and homoclinic tangencies. In principle, only two most important cases remain unproven: these are one-parameter families which unfold generally symmetric quadratic and cubic homoclinic tangencies. For both cases, the key problem is to find and study *symmetry-breaking bifurcations* in the first return maps.

One can standardly prove that these first return maps can be presented (in some rescaled coordinates and parameters) [GG09, DGG14, DGG15, GGO17] as reversible maps close to the conservative quadratic and cubic Hénon maps of the form $\bar{x} = y$, $\bar{y} = M - x - y^2$ and $\bar{x} = y$, $\bar{y} = -x + My \pm y^3$, respectively. These maps are reversible with respect to the involution $h : x \to y, \ y \to x$, and their dynamics has been studied for a long time. However, until recently, their symmetry-breaking bifurcations have been completely unknown. As for the conservative quadratic Hénon map, only in the very recent paper [GGS21], it has been shown that symmetry-breaking bifurcations occur starting with only 6-periodic orbits.

It is not the case of the cubic Hénon maps (1), where, as was shown in [DM00], symmetry-breaking bifurcations can take place for 3-periodic orbits which emerge near the degenerate 1:3 resonance. Moreover, in [DM00], the corresponding bifurcation diagrams were constructed. In Sections 3 and 4, we complement these diagrams providing phase portraits corresponding to transitions through bifurcation curves near the degenerate 1:3 resonance. Nevertheless, the main goal of the current paper is the study of peculiarities of *reversible symmetry-breaking bifurcations* associated with the 1:3 resonance in the cubic Hénon maps (1) under reversible non-conservative perturbations, see Sections 6, 7 and 8.

Recall that for reversible systems, typical (codimension 1) local symmetry-breaking bifurcations are supercritical and subcritical pitchfork bifurcations [LT12]. As a result of a supercritical bifurcation, a symmetric elliptic periodic orbit bifurcates into a saddle and in its neighborhood a symmetric pair of stable and unstable periodic orbits emerges, see Figure 2a-b. Under a subcritical bifurcation, the saddle periodic orbit becomes elliptic and there appears a symmetric pair of saddle periodic orbits, one with the Jacobian $J < 1$ and the other with the Jacobian $J > 1$, see Figure 2c-d. It is important to note that local symmetry-breaking bifurcations can be considered as an indicator of mixed dynamics in systems where the difference between intersecting attractor and repeller is invisible in standard numerics, for instance as in the nonholonomic model of rubber disk on the plane [GGK20].

Concerning global symmetry-breaking bifurcations, they are related to the appearance of non-transversal intersections between invariant manifolds of either the same periodic saddle orbit (homoclinic tangencies) or different saddles (heteroclinic tangencies). Under certain conditions bifurcations of these tangencies lead to the emergence of symmetric pairs of sinks and sources, area-expanding and area-contracting saddles as well as symmetric elliptic and saddle periodic orbits, and, hence, to the reversible mixed dynamics. Some of such global symmetry-breaking bifurcations were studied for non-transversal heteroclinic cycles of different types [GST97, LS04, DGGLS13, GGS20], see some examples of such cycles in Figure 1.

3 Construction of reversible non-conservative perturbations

Following ideas of [GGS21] we construct reversible non-conservative perturbations in the following conservative polynomial diffeomorphisms of the plane

$$H_n : \ \bar{x} = y, \quad \bar{y} = -x + P_n(y),$$

where $P_n(y)$ is a polynomial of degree n. These maps are also called *Hénon-like maps*. In particular, they include the cubic conservative Hénon maps for $P_3(y) = M_1 + M_2 y \pm y^3$.
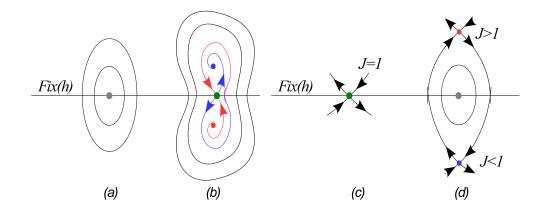
Figure 2: Two types of reversible pitchfork bifurcation: (a)→(b) supercritical pitchfork bifurcation at which an elliptic orbit (in plot (a)) becomes a saddle orbit and a pair of stable and unstable orbits appears near the saddle (in plot (b)); (c)→(d) subcritical pitchfork bifurcation at which a saddle orbit (in plot (c)) bifurcates into an elliptic orbit surrounded by a couple of saddle orbits with the Jacobians $J > 1$ and $J < 1$ (in plot (d)).

The first approach to get reversible non-conservative perturbations is based on the fact that the second iteration of the inverse conservative cubic Hénon maps $H_3^{\pm}$ can be implicitly presented in the reversible cross-form

$$f : (x, y) \to (\bar{x}, \bar{y}) : \quad \bar{x} = F(x, \bar{y}), \quad y = F(\bar{y}, x), \tag{2}$$

for which it is easy to add such perturbations. Indeed, the map (2) is reversible with respect to the involution $h : (x, y) \to (y, x)$, since $h \circ f \circ h : \quad \bar{y} = F(y, \bar{x}), \quad x = F(\bar{x}, y)$, and the inverse of this map coincides with (2). Thus, the map $\bar{y} = F(x, \bar{y}) + \epsilon(x, \bar{y}), y = F(\bar{y}, x) + \epsilon(\bar{y}, x)$ with an arbitrary smooth function ϵ is also reversible.

If $F(x, y)$ in the right hand side of (2) is linear in x, i.e. $F(x, y) = xG_1(y) + G_0(y)$, the map (2) can be rewritten in the explicit form

$$f : \quad \bar{x} = xG_1(\bar{y}) + G_0(\bar{y}), \quad \bar{y} = \frac{y - G_0(x)}{G_1(x)}. \tag{3}$$

If G_0 and G_1 are differentiable and $G_1(y) \neq 0, y \in \mathbb{R}$, the map (3) is a diffeomorphism. Indeed, the Jacobian of (3) is $J(f) = G_1(\bar{y})/G_1(x)$, which is different from 0, since $G_1 \neq 0$.

If we take $F(x, y) = -x + P_n(y) + \varepsilon\varphi(x, y)$, where ε is a small parameter and $\varphi(x, y)$ is a function (preferably linear in x) such that (2) is non-conservative, we get

$$\tilde{H}_n^2(\varepsilon) : \quad \bar{x} = -x + P_n(\bar{y}) + \varepsilon\varphi(x, \bar{y}), \quad y = -\bar{y} + P_n(x) + \varepsilon\varphi(\bar{y}, x), \tag{4}$$

which is a reversible perturbation of the second iteration of the inverse Hénon-like maps H_n^{-2}. This follows from the following lemma.

Lemma 1. *For $\varepsilon = 0$, the diffeomorphism $\tilde{H}_n^2(\varepsilon)$, defined in (4), satisfies the following property:*

$$\tilde{H}_n^2(0) = (H_n)^{-1} \circ (H_n)^{-1}.$$

Proof. We write the inverse map $(H_n)^{-1}$ (solving the equations in (3) for x and y and swapping $\bar{x} \leftrightarrow x, \bar{y} \leftrightarrow y$) as

$$(H_n)^{-1} : \quad \bar{x} = -y + P_n(x), \quad \bar{y} = x.$$

7

The second iteration of this map

$$(H_n)^{-2} = (H_n)^{-1} \circ (H_n)^{-1} : \quad \bar{x} = -x + P_n(-y + P_n(x)), \quad \bar{y} = -y + P_n(x)$$

coincides with $\tilde{H}_n^2(0)$. $\qquad\qquad\qquad\qquad\qquad\qquad\qquad\qquad\qquad\qquad\qquad\qquad$ $\square$

Recall that the bifurcation diagrams of H_n itself and the inverse map H_n^{-1} are related in the sense that an attractor of one map is a repeller of the other map and vice versa. Moreover, $\tilde{H}_n^2(0)$ appears while studying bifurcations of heteroclinic cycles connecting a saddle with the Jacobian $J > 1$ and a saddle with $J < 1$, see Figure 1.

In the case of the cubic polynomials $P_3(y) = M_1 + M_2 y \pm y^3$, the map (4) is the perturbed second iteration of the inverse cubic conservative Hénon map $H_3^{\pm}$

$$\tilde{H}_3^{\pm}(\varepsilon) : \bar{x} = M_1 + M_2 \bar{y} \pm \bar{y}^3 - x + \varepsilon\varphi(x, \bar{y}), \quad y = M_1 + M_2 x \pm x^3 - \bar{y} + \varepsilon\varphi(\bar{y}, x). \qquad (5)$$

In [SSK17] a numerical study of bifurcations of 1:3 and 1:4 resonances was done for the perturbed system $\tilde{H}_3^{2+}$ choosing $\varphi(x, y) = xy$. For the convenience of the reader, we include these results in Section 6. We also provide the same analysis for the perturbation $\tilde{H}_3^{2-}$ with $\varphi(x, y) = xy$ in Section 7.

In the case of the map (4), assuming the perturbation $\varphi(x, y) = x\varphi_1(y) + \varphi_0(y)$ is linear in the first variable x, we can study the explicit map

$$\tilde{H}_n^2(\varepsilon) : \quad \bar{x} = -x + P_n(\bar{y}) + \varepsilon\varphi(x, \bar{y}), \quad \bar{y} = \frac{-y + P_n(x) + \varepsilon\varphi_0(x)}{1 - \varepsilon\varphi_1(x)}.$$

Let us consider the perturbation $\varphi(x, y) = xy$. In particular, the cubic map $\tilde{H}_3^{2\pm}(\varepsilon)$, given in (5), turns out

$$\tilde{H}_3^{2\pm}(\varepsilon) : \quad \bar{x} = M_1 + M_2 \bar{y} \pm \bar{y}^3 - x + \varepsilon x\bar{y}, \quad \bar{y} = \frac{M_1 + M_2 x \pm x^3 - y}{1 - \varepsilon x}. \qquad (6)$$

For $\varepsilon = 0$, the map $\tilde{H}_3^{2\pm}(0)$ is the composition $(H_3^{\pm})^{-1} \circ (H_3^{\pm})^{-1}$ due to Lemma 1, hence, it is reversible and conservative. Also the perturbed map (6) is reversible with respect to the involution $h : (x, y) \to (y, x)$ due to the cross-form presentation. However, for $\varepsilon \neq 0$, the map $\tilde{H}_3^{2\pm}(\varepsilon)$ is not conservative anymore since the Jacobian of the map is not equal to 1:

$$J = \frac{1 - \varepsilon\bar{y}}{1 - \varepsilon x} \neq 1.$$

Therefore, one can consider the map (6) as a non-conservative perturbation of $(H_3^{\pm})^{-1} \circ (H_3^{\pm})^{-1}$ that preserves the reversibility.

The second method consists in writing the perturbations in the form

$$\tilde{H}_n(\varepsilon) : \quad \bar{x} + \varepsilon\varphi(\bar{y}, \bar{x}) = y + \varepsilon\varphi(x, y), \quad \bar{y} = -x + P_n(y + \varepsilon\varphi(x, y)), \qquad (7)$$

where ε is a small parameter and φ is a smooth function which gives a non-conservative perturbation. This perturbation can be obtained applying the so-called Quispel-Roberts method [QR92], see also [GGS21, BCR15]. This method uses two facts: (i) any two-dimensional reversible map f can be presented as the composition of two involutions, $f = \zeta_1 \circ \zeta_2$, and a perturbed map is obtained perturbing one of the involutions, $\tilde{f} = \zeta_1 \circ \tilde{\zeta}_2$; (ii) if ζ is an involution of f and the map T is a diffeomorphism, then $\tilde{\zeta} = T^{-1} \circ \zeta \circ T$ is also involution of f. Indeed, $H_n = h \circ h_1$, where $h : (x, y) \to (y, x)$, $h_2 : (x, y) \to (-x + P_n(y), y)$ are involutions. Thus, $\tilde{H}_n = h \circ \tilde{h}_2$ is obtained perturbing the second involution $\tilde{h}_2 = \tilde{h}_2 = T^{-1} \circ h_2 \circ T$ with a near identity map $T : \bar{x} = x, \bar{y} = y + \varepsilon\varphi(x, y)$.

8

Lemma 2. *The diffeomorphism $\tilde{H}_n(\varepsilon)$, defined in (7), is reversible with respect to the involution h :* $(x, y) \to (y, x)$.

Proof. The proof is similar to the one done in [DGGLS13] for the map (2), see also [GGS21]. Indeed, to prove the reversibility of $\tilde{H}_n(\varepsilon)$, we have to show that $\tilde{H}_n(\varepsilon)^{-1} = h \circ \tilde{H}_n(\varepsilon) \circ h$.

First, we write the inverse map $\tilde{H}_n(\varepsilon)^{-1}$ swapping the bar and no-bar variables $\bar{x} \leftrightarrow x, \bar{y} \leftrightarrow y$:

$$\tilde{H}_n(\varepsilon)^{-1} : \quad \bar{x} = -y + P_n(x + \varepsilon\varphi(y, x)), \quad \bar{y} + \varepsilon\varphi(\bar{x}, \bar{y}) = x + \varepsilon\varphi(y, x). \tag{8}$$

Second, the composition $\tilde{H}_n(\varepsilon) \circ h$ is obtained interchanging the variables $x \to y$, $y \to x$ in $\tilde{H}_n(\varepsilon)$ according to the involution h

$$\tilde{H}_n(\varepsilon) \circ h : \quad \bar{x} + \varepsilon\varphi(\bar{y}, \bar{x}) = x + \varepsilon\varphi(y, x), \quad \bar{y} = -y + P_n(x + \varepsilon\varphi(y, x)).$$

Then we apply h onto $\tilde{H}_n(\varepsilon) \circ h$ swapping the bar variables $\bar{x} \to \bar{y}$, $\bar{y} \to \bar{x}$ and get $h \circ \tilde{H}_n(\varepsilon) \circ h$ which coincides with $\tilde{H}_n(\varepsilon)^{-1}$ in (8). $\square$

For $\varepsilon = 0$, the map (7) coincides with the conservative map (3), not with the second iteration of the inverse map as in the first method. We consider the concrete perturbation $\varphi(x, y) = xy$

$$\tilde{H}_3^{\pm}(\varepsilon) : \quad \bar{x} + \varepsilon\bar{x}\bar{y} = y + \varepsilon xy, \quad \bar{y} = -x + M_1 + M_2(y + \varepsilon xy) \pm (y + \varepsilon xy)^3. \tag{9}$$

Since we choose a perturbation linear in the first variable x, the equations in (9) can be solved for $\bar{x}$ and $\bar{y}$. Thus, the maps $\tilde{H}_3^{\pm}$ can be written in the explicit form. The Jacobian of the maps equals

$$J = \frac{1 + \varepsilon x}{1 + \varepsilon\bar{y}}$$

which is different from 1 for $\varepsilon \neq 0$. We analyze numerically the bifurcations of the 1:3 resonance in the perturbed cubic conservative Hénon maps $\tilde{H}_3^d(\varepsilon)$ for $\varepsilon \neq 0$ and construct the corresponding bifurcation diagrams in Sections 6 and 7 paying special attention to the appearance of nonsymmetric periodic orbits under reversible pitchfork bifurcations.

Remark 1. *The maps (6) and (9) are not diffeomorphisms in the whole plane $\mathbf{R}^2$. However, the dynamics of this map is concentrated close to the origin, and for small ε the map can be considered as a diffeomorphism in a quite large neighborhood of the origin. Besides, for the first method, to have truly diffeomorphisms one can choose the perturbation $\varphi(x, y) = x\arctan(y)$ instead of $\varphi(x, y) = xy$.*

4   1:3 resonance for the unperturbed maps $H_3^{\pm}$

In the general non-conservative setting, the analysis of the 1:3 resonance was done by Arnold [Arn88], see also [AKN06, Kuz95]. For the study of the 1:3 resonance in conservative maps we refer to [BHJVW03, SV09]. Recall that one can study the structure of such bifurcations writing the local normal form expressed in complex coordinates $z = x + iy$ and $z^* = x - iy$:

$$\bar{z} = e^{i2\pi/3}(z + a_{02}(z^*)^2 + a_{21}z^2z^*) + O(|z|^4), \tag{10}$$

where the coefficient a_{02} is purely imaginary since map (10) is reversible with respect to the involution $h : z \to z^*$. In this case the 1:3 resonance is degenerate when $a_{02} = 0$.
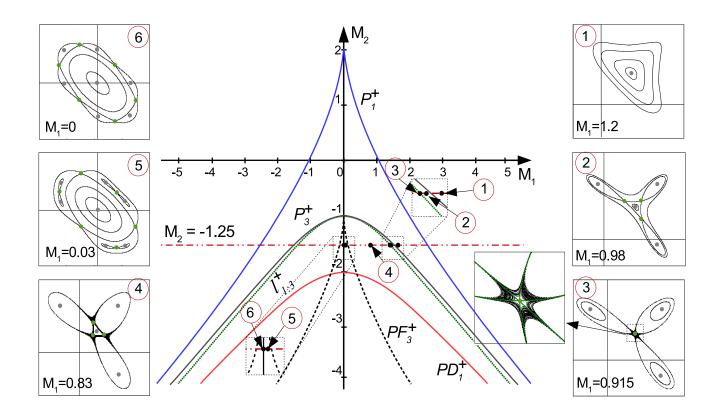
9

Figure 3: Bifurcation diagram for the conservative cubic Hénon map H_3^+. The bifurcations curves P_1^+, $l_{1:3}^+$, and PD_1^+ are the curves of a parabolic (pitchfork for $M_1 = 0$) bifurcation, 1:3 resonance, and a period-doubling bifurcation of fixed points, respectively. The curves P_3^+ and PF_3^+ are the curves of parabolic and pitchfork bifurcations of 3-periodic orbits, respectively. For the fixed value of $M_2 = -1.25$, the phase portraits are presented for $M_1 = 0, 0.03, 0.83, 0.915, 0.98$ and 1.2. For $M_1 < 0$ the phase portraits are reflected symmetrically with respect to $y = -x$.

Let $d = \pm 1$ be the coefficient before the cubic term in (1), thus, $d = 1$ corresponds to H_3^+ and $d = -1$ stands for H_3^-. Then, for the parameters M_1 and M_2 in the 1:3 resonance curve

$$l_{1:3}^d : M_1^2 = \frac{d}{27}(1 + M_2)(2M_2 - 7)^2, \tag{11}$$

the map H_3^d has the fixed point with eigenvalues $e^{\pm i 2\pi/3}$ which is $P_{1:3}^{(1)} = \sqrt{-d(1 + M_2)/3}\,(1, 1)$ in the branch $M_1 > 0$ and $P_{1:3}^{(2)} = -\sqrt{-d(1 + M_2)/3}\,(1, 1)$ in the branch $M_1 < 0$. Note that the curve $l_{1:3}^-$ has a self-intersection point at $(M_1, M_2) = (0, 7/2)$ where the map H_3^- has two fixed points $P_{1:3}^{(1)} = \left(\sqrt{3/2}, \sqrt{3/2}\right)$ and $P_{1:3}^{(2)} = \left(-\sqrt{3/2}, -\sqrt{3/2}\right)$ with eigenvalues $e^{\pm i 2\pi/3}$ simultaneously.

The coefficients of the normal form (10) are as follows:

$$\begin{aligned}
a_{02} &= -2i\sqrt{-d(1 + M_2)}, & \text{for } M_1 > 0, \\
a_{02} &= 2i\sqrt{-d(1 + M_2)}, & \text{for } M_1 < 0, \\
a_{21} &= -4d(1 + M_2) + 4\sqrt{3}dM_2 i.
\end{aligned}$$

It is easy to see that a_{02} and a_{21} do not vanish simultaneously. Moreover, $a_{02} = 0$ at $M_2 = -1$, therefore the 1:3 resonance is degenerate when $M_1 = 0, M_2 = -1$.
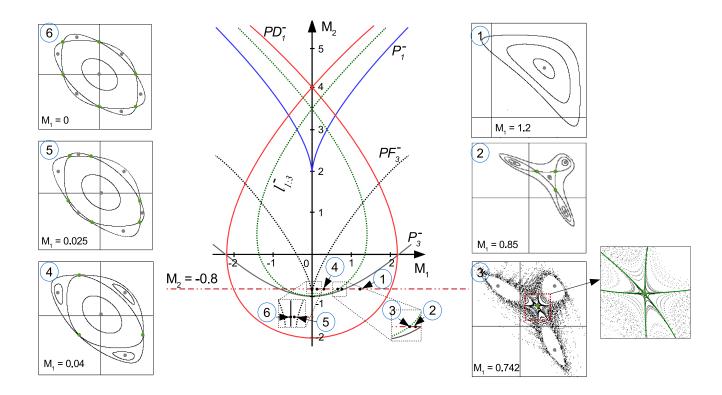
Figure 4: Bifurcation diagram for the conservative cubic Hénon map H_3^-. The bifurcations curves P_1^-, $l_{1:3}^-$, and PD_1^- are the curves of parabolic (pitchfork for $M_1 = 0$) bifurcation, 1:3 resonance, and period-doubling bifurcation of fixed points, respectively. The curves P_3^- and PF_3^- are the curves of parabolic and pitchfork bifurcations of 3-periodic orbits, respectively. The sequence of phase portraits in the horizontal line $M_2 = -0.8$ is displayed for $M_1 = 0, 0.025, 0.04, 0.742, 0.85$, and 1.2. For $M < 0$ the phase portraits are reflected symmetrically with respect to $y = -x$.

A detailed bifurcation analysis for the conservative cubic Hénon maps $H_3^{\pm}$ was carried out in [DM00, GGO17, GGOV18]. In particular, bifurcations of 3-periodic orbits were studied in [DM00], and one of the principal bifurcations were pitchfork bifurcations. For convenience, we display the corresponding bifurcation diagrams for H_3^+ and H_3^- and complement them with the related phase portraits in Figures 3 and 4, respectively.

Let us briefly describe these figures. Besides the 1:3 resonance curve $l_{1:3}^d$, defined in (11), the further bifurcation curves are P_1^d, PD_1^d, P_3^d and PF_3^d. The curves P_1^d and PD_1^d, which have the following equations

$$P_1^d: \qquad M_1^2 = \frac{4d}{27}(2 - M_2)^3$$
$$PD_1^d: \quad M_1^2 = -\frac{4d}{27}(2 + M_2)(4 - M_2)^2,$$

are the curves of fixed points with double eigenvalue (1,1) and (-1,-1), respectively. The curve P_1^d corresponds to a parabolic bifurcation of a fixed point of the map for $M_1 \neq 0$, $M_2 \neq 2$. As a result of this bifurcation, crossing P_1^d laterally, there appear elliptic and saddle (hyperbolic) fixed points for parameters below P_1^+ in the case of the map H_3^+ and above P_1^- in the case of the map H_3^-. When passing through the point $M_1 = 0$, $M_2 = 2$ at P_1^d vertically (being $M_1 = 0$ fixed) a subcritical and supercritical conservative pitchfork bifurcation takes place for H_3^+ and H_3^-, respectively. Namely, in the case of H_3^+, under this bifurcation the saddle fixed point for $M_2 > 2$ (above P_1^+) becomes elliptic and a pair of saddle fixed points appears around for $M_2 < 2$. For the map H_3^-, passing through the

point $M_1 = 0$, $M_2 = 2$ from bottom to top, an elliptic fixed point undergoes a supercritical pitchfork bifurcation, it turns into a saddle fixed point and a pair of elliptic fixed points appears nearby. The curve PD_1^d is related to a period-doubling bifurcation of a fixed point. At crossing PD_1^+, the elliptic fixed point becomes saddle and in its neighborhood there appears an elliptic 2-periodic orbit. The curve PD_1^- corresponds for two different types of period-doubling bifurcation: the bottom part is responsible for a subcritical period-doubling bifurcation of saddle fixed point (which becomes an elliptic fixed point surrounded by a saddle 2-periodic orbit), while at the upper part of PD_1^-, an elliptic fixed point undergoes a supercritical period-doubling bifurcation. See [GGO17] for more details on these bifurcations. The other curves P_3^d and PF_3^d are associated with parabolic and conservative pitchfork bifurcations of 3-periodic orbits, respectively. They were discovered by [DM00] and they have too cumbersome expressions to be presented, so we omit their equations.

We note that the point $(M_1, M_2) = (0, -1)$, corresponding to the case $a_{02} = 0$, is the cusp point of the curves PF_3^+ and PF_3^- in both maps H_3^+ and H_3^-, respectively. This point also lies in P_3^d and $l_{1:3}^d$. Getting inside the region bounded by the curve PF_3^+ (PF_3^-), the symmetric elliptic (saddle) 3-periodic orbit becomes saddle (elliptic) and a pair of nonsymmetric elliptic (saddle) orbits of the same period emerges for H_3^+ (H_3^-). It is worth mentioning that in the nonconservative reversible case, instead of nonsymmetric elliptic (saddle) orbits, a pair of stable and unstable orbits (saddles with the Jacobians $J > 1$ and $J < 1$) emerges as a result of a reversible pitchfork bifurcation.

In Figure 3 we present a sequence of phase portraits near the 1:3 resonance for a fixed M_2 for H_3^+. Let us give some details of the bifurcations which take place in the horizontal line $M_2 = -1.25$. For M_1 on the right hand side of the right branch of P_3^+ (see phase portrait ① for $M_1 = 1.2$), there is an elliptic fixed point E_1 which is born along with a saddle fixed point (the latter is not presented in the phase portrait) after a parabolic bifurcation at P_1^+. At crossing P_3^+ a parabolic bifurcation of 3-periodic orbits occurs and close to the elliptic point E_1 there appear 3-periodic orbits E_3 and S_3 of elliptic and saddle type, respectively, in the right hand side of P_3^+ (see, for example, phase portrait ② for $M_1 = 0.98$). In the 1:3 resonance curve $l_{1:3}$, the saddle 3-periodic orbit S_3 collides with the elliptic point E_1 and they become the saddle fixed point $P_{1:3}^{(1)}$ with 6 separatrices (see phase portrait ③ for $M_1 \approx 0.915$). After this bifurcation, the saddle 3-periodic orbit S_3 is reconstructed, and the homoclinic connections are transformed into heteroclinic cycles (see phase portrait ④ for $M_1 = 0.83$). At passage through the left curve PF_3^+ the elliptic 3-periodic orbit E_3 undergoes a supercritical pitchfork bifurcation: it becomes saddle $\hat{S}_3$ and a pair of nonsymmetric elliptic 3-periodic orbits $\hat{E}_3^1$ and $\hat{E}_3^2$ appears nearby (see, for instance, phase portrait ⑤ for $M_1 = 0.03$). Then the elliptic orbits $\hat{E}_3^1$ and $\hat{E}_3^2$ move away from $\hat{S}_3$ and get closer to S_3. At the same time, the separatrices of interior saddle $\hat{S}_3$ increase until they connect with the separatrices of the exterior saddle S_3 (the phenomenon of splitting of separatrices takes place). After some bifurcation related with homo/heteroclinic connections (phase portrait ⑥ at $M_1 = 0$) the saddle and elliptic 3-periodic orbits are rotated. Afterwards, by the symmetry in the (M_1, M_2)-plane, for $M_1 > 0$, the periodic orbits undergo an inverse pitchfork bifurcation (the elliptic 3-periodic orbits $\hat{E}_3^1$ and $\hat{E}_3^2$ merge into the saddle orbit S_3 which becomes elliptic E_3) at PF_3^+; a 1:3 resonance bifurcation (the saddle 3-periodic orbit $\hat{S}_3$ is reconstructed after passing through the saddle fixed point $P_{1:3}^{(2)}$ with 6 separatrices) takes place at $l_{1:3}^+$; an inverse parabolic bifurcation (the saddle and elliptic 3-periodic orbits E_3 and $\hat{S}_3$ merge into the elliptic fixed point E_1) occurs at crossing P_3^+.

In Figure 4 one can observe the bifurcations which occur at crossing the curves $l_{1:3}^-$, P_3^- and PF_3^- in the case of the map H_3^-. We consider the horizontal line $M_2 = -0.8$. For M_1 in the right hand side of P_3^- (see, for example, phase portrait ① for $M_1 = 1.2$), there are an elliptic fixed point E_1 and a saddle 2-periodic orbit (the latter is absent in the figure) which appear after a period-doubling bifurcation at PD_1^-. Decreasing M_1 and passing through the curve P_3^-, elliptic and

saddle 3-periodic orbits E_3 and S_3 show up surrounding the elliptic fixed point E_1 (see, for instance, phase portrait ② for $M_2 = 0.85$). Further, for M_1 in the curve $l_{1:3}^-$ the elliptic point E_1 and the saddle orbit S_3 are transformed into the saddle point $P_{1:3}^{(1)}$ with 6 separatrices (see phase portrait ③ at $M_1 \approx 0.74245$), and after crossing $L_{1:3}^-$ the saddle 3-periodic orbit S_3 is rotated reconstructing the homoclinic configuration into the heteroclinic connections (see phase portrait ④ for $M_1 = 0.04$). After that at crossing the right branch of PF_3^-, the saddle 3-periodic orbit S_3 goes through a subcritical pitchfork bifurcation: the saddle orbit becomes elliptic $\hat{E}_3$ and in its neighborhood there appear two nonsymmetric saddle 3-periodic orbits $\hat{S}_3^1$ and $\hat{S}_3^2$ (as in phase portrait ⑤ at $M_1 = 0.025$). Varying further M_1 the nonsymmetric saddle orbits $\hat{S}_3^1$ and $\hat{S}_3^2$ move away from the elliptic orbit $\hat{E}_3$ toward the other elliptic orbit E_3 (see, for instance, phase portrait ⑥ for $M_1 = 0$). For $M_1 < 0$, the two saddle orbits $\hat{S}_3^1$ and $\hat{S}_3^2$ get closer to E_3. These three orbits undergo an inverse pitchfork bifurcation while crossing the left branch of PF_3^-: the two saddle and elliptic 3-periodic orbits $\hat{S}_3^1$, $\hat{S}_3^2$ and $\hat{E}_3$ collide into the saddle 3-periodic orbit S_3. At crossing the left branch of $l_{1:3}^-$, the rotation of the saddle 3-periodic orbit S_3 takes place. Finally, for the parameters in the curve P_3^- the 3-periodic orbits $\hat{E}_3$ and S_3 disappear and the elliptic fixed point E_1 remains.

Remark 2. *The phase portraits in Figures 3 and 4 for values of parameters (M_1, M_2) and $(-M_1, M_2)$ are central symmetric with respect to the origin $x = y = 0$. This is due to the fact that the maps (1) are invariant under the change $x \to -x, y \to -y, M_1 \to -M_1$. This also results in the symmetries of the bifurcation curves in the (M_1, M_2) parameter plane with respect to $M_1 = 0$.*

Remark 3. *In Figures 3 and 4, the saddle separatrices are shown coinciding for simplicity, although they are not expected to be exactly merged since the phenomenon of splitting of separatrices occurs (see, for instance, [DGG16, DGG20] and references therein for more details about this phenomenon).*

5   On the degeneracy of the $p : q$ resonances with odd $q > 3$ in $H_3^\pm$ with $M_1 = 0$.

Let us consider the conservative cubic Hénon maps with $M_1 = 0$. Due to Remark 2, there is the central symmetry in the phase portraits $x \to -x, y \to -y$. A normal form for the $p : q$ resonance, where p and q are mutually prime and $q > 3$ is odd, is as follows

$$\bar{z} = e^{i2\pi p/q}(z + \Omega(|z|^2)z^* + A(z^*)^{q-1} + Bz^{q+1} + Cz(z^*)^q).$$

The corresponding flow normal form in this case can be written as follows:

$$\dot{z} = iz + \Omega(|z|^2)z^* + A(z^*)^{q-1} + Bz^{q+1} + Cz(z^*)^q. \tag{12}$$

It is conservative and reversible with respect to the involution $(t, z) \to (-t, z^*)$. Applying the involution gives

$$-\dot{z}^* = iz^* + \Omega(|z|^2)z + A(z)^{q-1} + B(z^*)^{q+1} + Cz^*(z)^q.$$

Further, let us consider the complex conjugate system

$$-\dot{z} = -iz + \Omega^*(|z|^2)z^* + A^*(z^*)^{q-1} + B^*(z)^{q+1} + C^*z(z^*)^q.$$

Thus, the reversibility implies that $\Omega = -\Omega^*, A = -A^*, B = -B^*, C = -C^*$, i.e. all coefficients in (12) should be pure imaginary. Therefore, equation (12) takes the form

$$\dot{z} = iz + i\Omega(|z|^2)z^* + iA(z^*)^{q-1} + iBz^{q+1} + iCz(z^*)^q, \tag{13}$$

where all coefficients Ω, A, B, C are real. The conservativity condition means zero divergence, i.e.

$$\frac{\partial \dot{z}}{\partial z} + \frac{\partial \dot{z}^*}{\partial z^*} \equiv 0$$

As it follows from (13)

$$\frac{\partial \dot{z}}{\partial z} = i + i\Omega'(z^*)^2 + i(q+1)Bz^q + iC(z^*)^q$$

and

$$\frac{\partial \dot{z}^*}{\partial z^*} = -i - i\Omega'(z)^2 - i(q+1)B(z^*)^q - iC(z)^q$$

Thus, the conservativity condition is

$$C + B(q+1) = 0.$$

The symmetry $z \to -z$ implies $A = B = C = 0$ since q is odd. Thus, the above condition is automatically fulfilled, and the following result holds.

Lemma 3. *For maps $H_3^{\pm}$ with $M_1 = 0$, any $p : q$ resonance at the fixed point $O(0,0)$, where $q > 3$ is odd, is at least triple degenerate.*

In Figure 5 we illustrate this result for both cubic Hénon maps $H_3^{\pm}$. In Figures 5a,b we show phase portraits near the degenerated 1:5 and 1:7 resonances for the map H_3^+. These resonances occur at $M_2 \approx 0.575$ and $M_2 \approx 1.15$, respectively. As a result, four periodic orbits emerge: a pair of symmetric periodic saddles (colored in light and dark green, respectively) and a pair of nonsymmetric periodic elliptic orbits (colored in grey and black, respectively). In Figure 5c,d we demonstrate phase portraits for the map H_3^-. In contrast to the previous case, here periodic elliptic orbits are symmetric while periodic saddles are nonsymmetric. Here the 1:5 resonance occurs at $M_2 \approx 0.66$ and the 1:7 resonance takes place at $M_2 \approx 1.36$.

6   On the 1:3 resonance for the perturbed maps $\tilde{H}_3^+(\varepsilon)$ and $\tilde{H}_3^{2+}$.

In this section we describe symmetry-breaking bifurcations near the 1:3 resonance in $\tilde{H}_3^+(\varepsilon)$ in the form (9). Note that the bifurcation picture is qualitatively similar for $\tilde{H}_3^{2+}(\varepsilon)$, defined in (6).

We apply reversible non-conservative perturbations to the conservative map H_3^+ and study their impact on the structure of the 1:3 resonance. We display the bifurcation diagram for the fixed perturbation parameter $\varepsilon = 0.05$ in Figure 6. In comparison to the unperturbed case, we can see the slightly changed bifurcation curves $l_{1:3}^+$, P_3^+ and PF_3^+, related to the 1:3 resonance, a parabolic bifurcation of the appearance of 3-periodic orbits and a reversible pitchfork bifurcation of 3-periodic orbits, respectively. Unlike the conservative case, the bifurcation curves are not symmetric since the invariance of the map with respect to the change $M_1 \to -M_1$ (see also Remark 2) is not conserved anymore at adding the perturbation. However, the symmetry in the phase portraits with respect to the straight line $y = x$ is preserved due to the reversibility. Also the curve PF_3^+ here is associated with the symmetry-breaking bifurcations which are non-conservative reversible pitchforks.

Let us describe the sequence of bifurcations which occur for the fixed parameter $M_2 = -1.25$ and decreasing the parameter M_1 in Figure 6. To the right hand side of the curve P_3^+ (see, for example, the phase portrait ① at $M_1 = 1.2$), the map $\tilde{H}_3^+(\varepsilon)$ (and also $\tilde{H}_3^{2+}$) has an elliptic fixed point E_1. At crossing P_3^+, there appear a symmetric elliptic 3-periodic orbit E_3 and a symmetric saddle 3-periodic
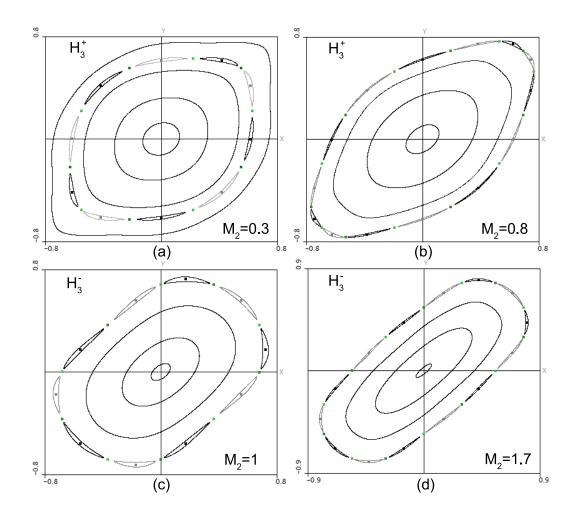
Figure 5: Phase portraits near the degenerated 1:5 (left column) and 1:7 (right column) resonances in the conservative cubic Hénon maps H_3^+ (top row) and H_3^- (bottom row).

orbit S_3 with homoclinic loops (see the phase portrait ② for the parameter value $M_1 = 0.96$). Then approaching the curve $l_{1:3}^+$, the orbits S_3 and E_1 merge into a saddle fixed point with 6 separatrices (phase portrait ③ at $M_1 \approx 0.882737$). After that the saddle splits into elliptic point E_1 and saddle 3-periodic orbit S_3, now S_3 is rotated and form heteroclinic connections (phase portrait ④ for $M_1 = 0.15$). Further, the elliptic 3-periodic orbit E_3 undergoes a reversible pitchfork bifurcation at crossing the right branch of the curve PF_3^+: the elliptic 3-periodic orbit E_3 breaks into saddle, stable and unstable 3-periodic orbits $\hat{S}_3$, $\hat{A}_3$ and $\hat{R}_3$, respectively (phase portrait ⑤ for $M_1 = 0.08$). Note that under this bifurcation a pair of nonsymmetric 3-periodic orbits $\hat{A}_3$ and $\hat{R}_3$ is born. The separatrices of each component of the new saddle $\hat{S}_3$ tend to the the corresponding components of the stable and unstable orbits $\hat{A}_3$ and $\hat{R}_3$ at forward and backward iterations, respectively, forming homoclinic loops, and all the three components are surrounded by invariant curves in the similar way as in Figure 2(a). Decreasing M_1, the stable and unstable orbits $\hat{A}_3$ and $\hat{R}_3$ move away from each other. Moreover, one of the components of the stable (or unstable) 3-periodic orbit gets away from the symmetry line $y = x$, while the other two components move closer each other and to the line $y = x$. At the same time, the separatrices of the inner saddles become larger. At some moment (close to $M_1 = 0.055$, see phase portrait ⑥), the separatrices of the inner and exterior saddles $\hat{S}_3$ and S_3 merge (not exactly due to splitting of separatrices) and the transformation of
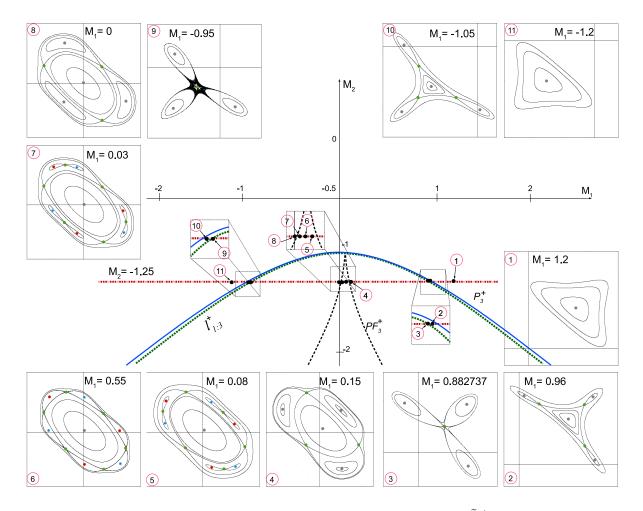
15

Figure 6: Bifurcation diagram for the reversible non-conservative map $\tilde{H}_3^+(\varepsilon)$ for $\varepsilon = 0.05$ near the 1:3 resonance. The bifurcations curve $l_{1:3}^+$ is the curve of the 1:3 resonance of fixed points, while the curves P_3^+ and PF_3^+ are related to parabolic and reversible pitchfork (non-conservative symmetry-breaking) bifurcations of 3-periodic orbits, respectively. For the fixed value of $M_2 = -1.25$, the phase portraits are given for $M_1 = -1.2, -1.05, -.95, 0, 0.003, 0.055, 0.08, 0.15, 0.8827, 0.96$ and 1.2. The green, grey, red and blue stand for saddle, elliptic, stable (sinks) and unstable (sources) fixed points and periodic orbits, respectively.

homoclinic/heteroclinic connections takes place after which all the involved 3-periodic orbits are rotated (as in phase portrait ⑦ for $M_1 = 0.03$). At crossing the left branch of PF_3^+ an inverse pitchfork bifurcation occurs: the saddle, stable and unstable 3-periodic orbits S_3, $\hat{A}_3$ and $\hat{R}_3$ merge into an elliptic 3-periodic orbit E_3 (phase portrait ⑧ at $M_1 = 0$). The remaining saddle 3-periodic orbit $\hat{S}_3$ and elliptic point E_1 collide at crossing the left branch of $l_{1:3}^+$, there is a saddle point with 6 separatrices for the parameters in this curve (for a parameter close to $M_1 = -0.95$, see phase portrait ⑨). After the bifurcation, the 6-separatrix saddle splits into saddle and elliptic 3-periodic orbits $\hat{S}_3$ and E_3 in the left hand side of $l_{1:3}^+$, now $\hat{S}_3$ is rotated by $\pi/3$ and the heteroclinic cycles change into homoclinic loops (phase portrait ⑩ for $M_1 = -1.05$). Finally, we transit the curve P_3^+ and the 3-periodic orbits $\hat{S}_3$ and E_3 disappear (phase portrait ⑪ for $M_1 = -1.2$).

Thus, at transition into the domain lying below the curve PF_3^+, there appears a symmetric pair of nonsymmetric stable and completely unstable 3-periodic orbits. This fact is relevant for detecting mixed dynamics in maps with symmetric cubic homoclinic tangencies whose truncated first return
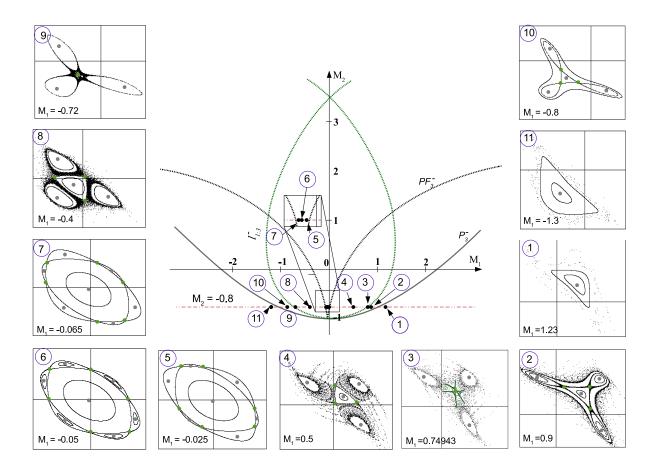
16

Figure 7: Bifurcation diagram for the the reversible non-conservative map $\tilde{H}_3^-(\varepsilon)$ for $\varepsilon = 0.05$ near the 1:3 resonance. The bifurcations curve $l_{1:3}^-$ is related to bifurcations of the 1:3 resonance of fixed points, while the curves P_3^- and PF_3^- correspond to parabolic and reversible pitchfork (non-conservative symmetry-breaking) bifurcations of 3-periodic orbits, respectively. For the fixed value of $M_2 = -0.8$, the phase portraits are given for $M_1 = -1.3, -0.8, -0.72, -0.4, -0.065, -0.005, -0.025, 0.5, 0.7494, 0.9$ and 1.23. The green and grey points stand for saddle and elliptic orbits, respectively.

map is $\tilde{H}_3^+(\varepsilon)$ or $\tilde{H}_3^{2+}(\varepsilon)$. Thus, there are Newhouse domains where maps with infinitely many attracting, repelling, saddle and elliptic periodic orbits are dense.

7 On the 1:3 resonance in the perturbed maps $\tilde{H}_3^-(\varepsilon)$ and $\tilde{H}_3^{2-}(\varepsilon)$

In this section we study how the 1:3 resonance evolves under the perturbation in the case of the map $\tilde{H}_3^-(\varepsilon)$. The corresponding bifurcation diagram is illustrated in Figure 7. Unlike the unperturbed case in Figure 4, the 1:3 resonance curve $l_{1:3}^-$ as well as the curves P_3^- and PF_3^- related to parabolic and reversible pitchfork bifurcations of 3-periodic orbits, respectively, are nonsymmetric and slightly moved, since the symmetry with respect to $M_1 = 0$ (see also Remark 2) is not conserved anymore. Also PF_3^- corresponds to a non-conservative symmetry-breaking bifurcation after which two nonsymmetric saddle 3-periodic orbits appear, one of them with the Jacobian $J > 1$ and the other with the Jacobian $J < 1$. Note that for $\tilde{H}_3^{2-}(\varepsilon)$, the bifurcation diagram and bifurcation sequence of phase portraits is qualitatively the same.

Let us give details on the bifurcations taking place in the bifurcation diagrams in Figure 7. We choose the horizontal line $M_2 = -0.8$. We start with the parameters in the right hand side of P_3^- (see, for instance, phase portrait ① for $M_1 = 1.23$), where the map $\tilde{H}_3^-(\varepsilon)$ (and $\tilde{H}_3^{2-}(\varepsilon)$) has an elliptic fixed point E_1. The point E_1 undergoes a parabolic bifurcation at crossing P_3^- and there appear 3-periodic orbits S_3 and E_3 of saddle and elliptic type close to E_1 for the parameters in the left hand side of P_3^- (phase portrait ② for $M_1 = 0.9$). Note that the three components of the saddle orbit S_3 have homoclinic loops. In the 1:3 resonance curve $l_{1:3}^-$ (at $M_1 \approx 0.74943$), the saddle 3-periodic orbit S_3 and the elliptic point E_1 merge into a saddle fixed point with 6 separatrices (see phase portrait ③) which for the parameters in the left hand side of $l_{1:3}^-$ breaks into saddle and elliptic 3-periodic orbits S_3 and E_3 again, but in the left hand side of $l_{1:3}^-$ the orbit S_3 is rotated by $\pi/3$ and the homoclinic loops of S_3 are reorganized into heteroclinic connections (see, for example, phase portrait ④ at $M_1 = 0.5$). Crossing the right branch of the curve PF_3^-, the saddle orbit S_3 undergoes the subcritical pitchfork bifurcation. As a result, the saddle orbit is converted into an elliptic 3-periodic orbit $\hat{E}_3$ and two saddle 3-periodic orbits $\hat{S}_3^1$ and $\hat{S}_3^2$ show up nearby (see the phase portrait ⑤ for $M_1 = -0.025$). Moreover, the Jacobian in $\hat{S}_3^1$ is greater than 1 and the Jacobian in $\hat{S}_3^2$ is less than 1. Decreasing the parameter M_1, the saddle orbits $\hat{S}_3^1$ and $\hat{S}_3^2$ distance from each other and they move toward the elliptic orbit E_3 (phase portraits ⑥ and ⑦ for $M_1 = -0.05$ and $M_1 = -0.065$). In the left branch of PF_3^-, an inverse pitchfork bifurcation takes place: the orbit E_3 merges along with $\hat{S}_3^1$ and $\hat{S}_3^2$ into a saddle 3-periodic orbit S_3 (phase portrait ⑧ for $M_1 = -0.4$). Afterwards, the reconstruction of S_3 happens in the 1:3 resonance curve $l_{1:3}^-$ (phase portrait ⑨ and ⑩ for $M_1 = -0.72$ and $M_1 = -0.8$). Finally, the 3-periodic orbits $\hat{E}_3$ and S_3 disappear at crossing P_3^- (phase portrait ⑪) for $M_1 = -1.3$.

Note that in the domain above the curve PF_3^- there emerges a symmetric pair of nonsymmetric saddle 3-periodic orbits whose Jacobians are greater and less than 1. This configuration also implies the existence of mixed dynamics in maps with cubic homoclinic tangencies whose truncated first return map is $\tilde{H}_3^-(\varepsilon)$ or $\tilde{H}_3^{2-}(\varepsilon)$. Also in $\tilde{H}_3^-(\varepsilon)$ itself we show numerically the existence of mixed dynamics for the parameters from the domain inside PF_3^- since heteroclinic connections between two saddle orbits, one with the Jacobian $J > 1$ and the other with the Jacobian $J < 1$, leads to the presence of the so-called Lamb-Stenkin non-transversal heteroclinic cycle [LS04]. See more details in Section 8.

8 Numerical evidence of mixed dynamics in the perturbed map $\tilde{H}_3^-(\varepsilon)$

In this section we provide a numerical evidence of the existence of mixed dynamics in the perturbed map $\tilde{H}_3^-(\varepsilon)$ in (9) for which in Section 7 we show the existence of a pair of saddle 3-periodic orbits $\hat{S}_3^1$ and $\hat{S}_3^2$ with the Jacobians $J < 1$ and $J > 1$, respectively. Recall that these orbits appear due to a subcritical reversible pitchfork bifurcation of the symmetric saddle 3-periodic orbit S_3. For better visibility, we take a quite large value of perturbation, $\varepsilon = 0.3$. In Figure 8 we show the phase portraits of $\tilde{H}_3^-(\varepsilon)$ for $M_1 = -0.364$ and $M_2 = -0.5$. The orbits $\hat{S}_3^1$ with $J < 1$, $\hat{S}_3^2$ with $J > 1$ and symmetric elliptic orbits are marked by blue, red and black bold points, respectively. For the convenience, we rotate the phase portraits by $\pi/4$, then the horizontal axis corresponds to $Fix(h)$.

From Figure 8 it is clear to see that the phase portrait is self-symmetric with respect to the horizontal axis which means that the attractor of the system seems coincident with the repeller. Moreover, we are not able to find periodic sinks and sources nor even nonsymmetric orbits (except for points $\hat{S}_3^1$ and $\hat{S}_3^2$) which would confirm mixed dynamics in $\tilde{H}_3^-(\varepsilon)$.

However, we find a non-transversal heteroclinic cycle of Lamb-Stenkin type [LS04] which con-
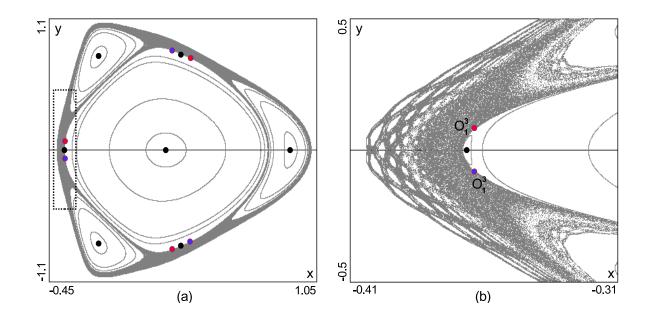
Figure 8: Phase portrait and the zoomed fragment for the map $\tilde{H}_3^-(\varepsilon)$ in (9) for $M_1 = -0.364$, $M_2 = -0.5$ and $\varepsilon = 0.3$. For the convenience, the phase portrait is rotated by $\pi/4$. In this representation, the horizontal axis becomes $Fix(h)$. The chaotic dynamics (in the gray region) seems conservative (the phase portrait is self-symmetric with respect to the horizontal axis). The orbits $\hat{S}_3^1$ and $\hat{S}_3^2$ are the pair of non-conservative saddle 3-periodic orbits with the Jacobians $J(\hat{S}_3^1) = 0.995 < 1$ and $J(\hat{S}_3^2) = 1.005 > 1$.

nects $\hat{S}_3^1$ and $\hat{S}_3^2$. As it was shown in [LS04], bifurcations of such cycles lead to a reversible mixed dynamics. A schematic representation of this cycle is shown in Figure 9a. The numerically obtained cycle is presented in Figure 9b. From this figure, one can see that the stable and unstable manifolds of $\hat{S}_3^1$ and $\hat{S}_3^2$ have both transversal (see also the zoomed region near $\hat{S}_3^2$ in Figure 9c) and non-transversal (see the zoomed fragment in Figure 9b) intersections. Thus, we can state that the chaotic dynamics presented in the gray zone in Figure 8 is mixed.

Also in this section we would like to note that the presence of mixed dynamics near elliptic points of two-dimensional reversible maps plays an important role. As well-known, the phase portrait near an elliptic point of a two-dimensional reversible diffeomorphism is organized in many details as in the conservative case. There is also a continuum of KAM-curves surrounding the elliptic point. The KAM-curves are separated by resonant zones [Sev86]. However, the behavior in the resonant zones for reversible maps principally differs from the conservative ones, see, for example, Figures 10a and 10b. In the conservative setting, ε-orbits can run away from any neighborhood of an elliptic point, i.e. such point is not stable under permanently acting perturbations (Lyapunov instability by ε-orbits) [GT17], see Figure 10a.

On the other hand, in the reversible nonconservative case, as it follows from [GLRT14, GT17], it is typical when in resonant zones periodic saddle points alternate with symmetric pairs of sinks and sources, see Figure 10(b). In this case, it is possible when there exist intersecting absorbing domain B_A and repelling domain B_R around an elliptic point such that forward as well as backward ε-orbits of any point, that belongs to the intersection $B_A \cap B_R$, cannot leave any neighborhood of this elliptic point [GT17, GGK20]. These resonances are called *impassable* or *isolated*. In future papers, we plan to study such resonances for the perturbed reversible non-conservative Hénon maps.
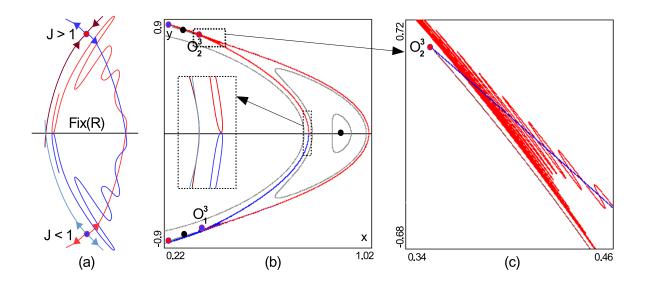
Figure 9: (a) A schematic representation of non-transversal heteroclinic cycle of Lamb-Stenkin type. (b), (c) Non-transversal heteroclinic cycle connected saddles $\hat{S}_3^1$ and $\hat{S}_3^2$ in the map $\tilde{H}_3^-(\varepsilon)$ at $M_1 = -0.364$, $M_2 = -0.5$ and $\varepsilon = 0.3$. A pair of manifolds W_1^s and W_1^u intersects transversally, while the other pair W_2^s and W_2^u has a quadratic tangency.

Conclusions

In the present paper we have obtained a series of new results devoted to the structure of the 1:3 resonance in conservative cubic Hénon maps and their reversible perturbations. First, we have used two methods to construct reversible non-conservative perturbations of the conservative cubic Hénon maps. The first method provides perturbations of the second iteration of the inverse cubic Hénon maps in the so-called cross-form, while the second more delicate method gives perturbations of the cubic Hénon maps themselves. In both cases, we have proved that the resulting perturbed perturbations preserve reversibility. Second, we have considered the conservative cubic Hénon maps H_3^+ and H_3^- as examples and studied the influence of reversible non-conservative perturbations on the structure of bifurcations of the 1:3 resonance. We have provided a detailed analysis of these bifurcations in the perturbed maps. We have focused on local symmetry-breaking bifurcations which have led to the appearance of nonsymmetric orbits. These bifurcations are reversible pitchfork bifurcations of 3-periodic orbits, and we have found the domains of parameters corresponding to nonsymmetric orbits. Moreover, for perturbations of H_3^+, there appear nonsymmetric asymptotically stable and completely unstable 3-periodic orbits, while in perturbed H_3^- there emerge two nonsymmetric saddle 3-periodic orbits, one with the Jacobian greater than 1 and the other with the Jacobian less than 1. The presence of these nonsymmetric orbits leads to the existence of mixed dynamics in maps with cubic homoclinic tangencies whose first return maps are $H_3^{\pm}$. Third, for the unperturbed conservative maps H_3^+ and H_3^- with $M_1 = 0$, we have demonstrated that all $p : q$ resonances are degenerate when $q > 3$ is odd. And finally, we have provided a numerical evidence of mixed dynamics in perturbed H_3^-, since a heteroclinic configuration between these nonsymmetric saddle orbits implies the emergence of a Lamb-Stenkin non-transversal heteroclinic cycle.

These results can be used for further study of mechanisms of the appearance of mixed dynamics after a break-down of conservative dynamics. As pointed out in the introduction, the maps (1) are related to the study of cubic homoclinic tangencies and the phenomenon of mixed dynamics, the third
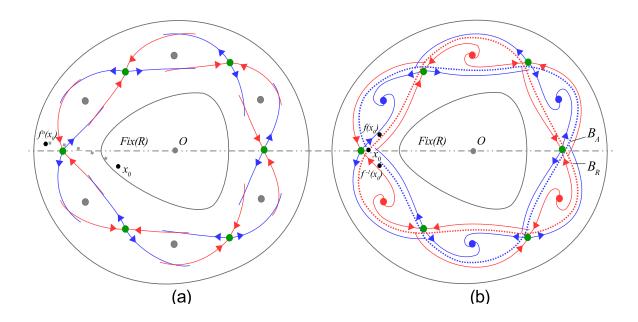
Figure 10: Different types of behavior in resonant zones of a symmetric elliptic point in the conservative (a) and reversible (b) cases. Periodic elliptic orbits are marked by gray bold points, while periodic sinks and sources are colored in blue and red, respectively. In plot (b) the absorbing domain B_A of a sink orbit (bounded by the blue dashed curves) intersects with the repelling domain of the source orbit (bounded by the red dashed curves). Thus, ε-orbits of any point belonging to this intersection cannot leave the resonant zone with neither forward nor backward iterations (isolated resonance). It means that an elliptic point of a typical two-dimensional reversible diffeomorphism is stable under permanently acting perturbations (Lyapunov stability by ε-orbits).

(and the last) type of chaos. We have shown some global and local mechanisms of its emergence. The global ones are connected with the presence of homoclinic and heteroclinic cycles of different kinds, while one of the interesting local mechanisms is related to bifurcations of resonances among which we highlight the 1:3 resonance. It is easy to associate the bifurcation structure of the cubic Hénon maps with the bifurcations which take place near the cubic homoclinic tangencies [GGO17]. In the present paper we have proposed a local mechanism corresponding to the occurrence of degenerate resonances in the cubic Hénon maps. In the reversible context, symmetry-breaking pitchfork bifurcations of 3-periodic orbits lead to the appearance of pairs of nonsymmetric and non-conservative periodic orbits (periodic sinks and sources, periodic saddles with the Jacobians greater and less than 1) near the degenerate 1:3 resonant point. In this regard, we think that it is of great importance to consider the problem of local 1:3 resonance, especially the degeneracy $a_{02} = 0$ in (10), and the accompanying symmetry-breaking bifurcations in general reversible maps, since degenerate resonances in reversible systems are the main local mechanism of the appearance of mixed dynamics. It is also worth mentioning that the similar problem for the 1:4 resonance, the structure of bifurcations associated with fixed points with eigenvalues $e^{\pm \pi/2} = \pm i$ and, consequently, 4-periodic orbits, is of great interest as well. An exhaustive study of 1:4 resonance for (1) was done in [GGO17, GGOV18], see also [Gon05]. It was also established in these works that for some (M_1, M_2), the 1:4 resonance can be degenerate and the 4-periodic orbits are subject to pitchfork bifurcations. The study of reversible non-conservative perturbations for this case is planned in a forthcoming paper.

Acknowledgments

References

[AB85] D. V. Anosov, I. U. Bronshtein. Smooth dynamical systems. Chapter 3. Itogi Nauki i Tekhniki. Seriya "Sovremennye Problemy Matematiki. Fundamental'nye Napravleniya", 1, 204-229, 1985.

[AKN06] V. I. Arnold, V. V. Kozlov, A. I. Neishtadt. Mathematical aspects of classical and celestial mechanics. [Dynamical systems. III]. Translated from the Russian original by E. Khukhro. Third edition. Encyclopaedia of Mathematical Sciences, 3. *Springer-Verlag*, Berlin, 2006.

[Arn88] V.I. Arnold. Geometrical Methods in the Theory of Ordinary Differential Equations. *Springer*; 2nd edition, 1988.

[AS20] G. Ariel, J. Schiff. Conservative, dissipative and super-diffusive behavior of a particle propelled in a regular flow. *Physica D: Nonlinear Phenomena*, p. 132584, 2020.

[BCR15] M. Bessa, M. Carvalho, Alexandre Rodrigues. Generic area-preserving reversible diffeomorphisms. *Nonlinearity*, 28(6):1695–1720, 2015.

[BHJVW03] H. Broer, H. Hanßmann, À Jorba, J. Villanueva, F. Wagener. Normal-internal resonances in quasi-periodically forced oscillators: a conservative approach. *Nonlinearity* 16(5):1751–1791, 2003.

[Bir87] V. S. Biragov. Bifurcations in a two-parameter family of conservative mappings that are close to the Hénon mapping. (Russian) [Translated in *Selecta Math. Soviet.* 9(3):273–282, 1990.] *Methods of the qualitative theory of differential equations*, 10–24, 1987

[BM20a] I. A. Bizyaev, I. S. Mamaev. Separatrix splitting and nonintegrability in the nonholonomic rolling of a generalized Chaplygin sphere. *International Journal of Non-Linear Mechanics*, 126:103550, 2020.

[BM20b] I. A. Bizyaev, I. S. Mamaev. Dynamics of the nonholonomic Suslov problem under periodic control: unbounded speedup and strange attractors. *Journal of Physics A: Mathematical and Theoretical*, 53(18):185701, 2020.

[Con78] C. C. Conley. Isolated invariant sets and the Morse index. *American Mathematical Soc.*, No. 38, 1978.

[DGG14] A. Delshams, M. Gonchenko, S.V. Gonchenko. On bifurcations of area-preserving and nonorientable maps with quadratic homoclinic tangencies. *Regular and Chaotic Dynamics*, 19(6):702-717, 2014.

[DGG15] A. Delshams, M. Gonchenko, S. Gonchenko. On dynamics and bifurcations of area-preserving maps with homoclinic tangencies. *Nonlinearity*, 28(9):3027–3071, 2015.

[DGG16] A. Delshams, M. Gonchenko, and P. Gutiérrez. Exponentially small splitting of separatrices and transversality associated to whiskered tori with quadratic frequency ratio. *SIAM J. Appl. Dyn. Syst.*, 15(2):981–1024, 2016.

[DGG20] A. Delshams, M. Gonchenko, P. Gutiérrez. Exponentially small splitting of separatrices associated to 3D whiskered tori with cubic frequencies. *Comm. Math. Phys.*, 378(3):1931-1976, 2020.

[DGGL18] A. Delshams, M. Gonchenko, S.V. Gonchenko, J.T. Lázaro. Mixed dynamics of two-dimensional reversible maps with a symmetric couple of quadratic homoclinic tangencies. *Discrete and Continuous Dynamical Systems*, 38(9):4483–4507, 2018.

[DGGLS13] A. Delshams, S. V. Gonchenko, V. S. Gonchenko, J. T. Lazaro, O. Stenkin. Abundance of attracting, repelling and elliptic periodic orbits in two-dimensional reversible maps. *Nonlinearity*, 26(1):1–33, 2013.

[DM00] H. R. Dullin, J. D. Meiss. Generalized Hénon maps: the cubic diffeomorphisms of the plane. *Physica D: Nonlinear Phenomena*, 143(1):262–289, 2000.

[GG09] S.V. Gonchenko, M.S. Gonchenko. On cascades of elliptic periodic points in two-dimensional symplectic maps with homoclinic tangencies. *Regular and Chaotic Dynamics*, 14(1):116–136, 2009.

[GGK13] A. S. Gonchenko, S. V. Gonchenko, A. O. Kazakov. Richness of chaotic dynamics in non-holonomic models of a Celtic stone. *Regular and Chaotic Dynamics*, 18(5):521–538, 2013.

[GGK20] S.V. Gonchenko, A.S. Gonchenko, A.O. Kazakov. On three types of attractors and mixed dynamics in nonholonomic models of rigid body dynamics. *Proceedings of the Steklov Institute of Mathematics* 2020. Vol. 308. pp. 125-140.

[GGKT17] A. S. Gonchenko, S. V. Gonchenko, A. O. Kazakov, D. V. Turaev. On the phenomenon of mixed dynamics in Pikovsky-Topaj system of coupled rotators. *Physica D: Nonlinear Phenomena*, 350:45–57, 2017.

[GGO17] M. Gonchenko, S. Gonchenko, I. Ovsyannikov. Bifurcations of cubic homoclinic tangencies in two-dimensional symplectic maps. *Mathematical Modelling of Natural Phenomena*, 12(1):41–61, 2017.

[GGOV18] M. Gonchenko, S. Gonchenko, I. Ovsyannikov, A. Vieiro. On local and global aspects of the 1:4 resonance in the conservative cubic Hénon maps *Chaos: An Interdisciplinary Journal of Nonlinear Science*, 28(4):043123 [15 pp], 2018.

[GGS21] M. S. Gonchenko, S. V. Gonchenko, K. Safonov. Reversible perturbations of conservative Hénon-like maps. *Discrete and Continuous Dynamical Systems*, 41(4): 1875-1895, 2021.

[GGS20] S. V. Gonchenko, M. Gonchenko, I. O. Sinitsky. On the mixed dynamics of two-dimensional reversible diffeomorphisms with symmetric heteroclinic contours (Russian). *Izvestiya Rossiiskoi Akademii Nauk. Seriya Matematicheskaya*, 84(1):23-51, 2020.

[GLRT14] S. V. Gonchenko, J. S. W. Lamb, I. Rios, D. Turaev. Attractors and repellers in the neighborhood of elliptic points of reversible systems. (Russian) *Dokl. Akad. Nauk*, 454(4):375–378, 2014; translation in *Dokl. Math.* 89(1):65-–67, 2014.

[Gon85] S.V. Gonchenko. On a two parameter family of systems close to a system with a nontransversal Poincaré homoclinic curve. I. (Russian) [Translated in *Selecta Math. Soviet.*, 10(1):69-80, 1991] *Methods of Qualitative Theory of Differential Equations*, 55-72, 1985.

[Gon05] M.S. Gonchenko. On the structure of 1:4 resonances in Hénon maps, *Internat. J. Bifur. Chaos Appl. Sci. Engrg*, 15(11):3653-3660, 2005.

[Gon16] S. Gonchenko. Reversible Mixed Dynamics: A Concept and Examples. *Discontinuity, Nonlinearity, and Complexity*, 5(4):345-–354, 2016.

[GST97] S. V. Gonchenko, L. P. Shilnikov, D. V. Turaev. On Newhouse domains of two-dimensional diffeomorphisms which are close to a diffeomorphism with a structurally unstable heteroclinic cycle. *Proc. Steklov Inst. Math.*, 216:70–118, 1997.

[GSV13] S.V. Gonchenko, C. Simo, A. Vieiro. Richness of dynamics and global bifurcations in systems with a homoclinic figure-eight. *Nonlinearity*, 26(3):621, 2013.

[GT17] S. Gonchenko, D. Turaev. On three types of dynamics, and the notion of attractor. *Trudy Matematicheskogo Instituta imeni V.A. Steklova*, 297:133–157, 2017.

[EN19] A. A. Emelianova, V. I. Nekorkin. On the intersection of a chaotic attractor and a chaotic repeller in the system of two adaptively coupled phase oscillators. *Chaos: An Interdisciplinary Journal of Nonlinear Science*, 29(11):111102, 2019.

[EN20] A. A. Emelianova, V. I. Nekorkin. The third type of chaos in a system of two adaptively coupled phase oscillators. *Chaos: An Interdisciplinary Journal of Nonlinear Science*, 30(5):051105, 2020.

[EN21] A. A. Emelianova, V. I. Nekorkin. Emergence and synchronization of a reversible core in a system of forced adaptively coupled Kuramoto oscillators. *Chaos: An Interdisciplinary Journal of Nonlinear Science*, 31(3):033102, 2021.

[Kaz13] A.O. Kazakov. Strange attractors and mixed dynamics in the problem of an unbalanced rubber ball rolling on a plane. *Regular and Chaotic Dynamics*, 18(5):508–520, 2013.

[Kaz19] A. O. Kazakov. On the Appearance of Mixed Dynamics as a Result of Collision of Strange Attractors and Repellers in Reversible Systems, *Radiophysics and Quantum Electronics*, pp. 1-9, 2019.

[Kaz20] A. Kazakov. Merger of a Hénon-like attractor with a Hénon-like repeller in a model of vortex dynamics. *Chaos: An Interdisciplinary Journal of Nonlinear Science*, 30(1):011105, 2020.

[Kuz95] Yu. Kuznetsov. Elements of applied bifurcation theory. Applied Mathematical Sciences, 112. *Springer-Verlag, New York*, 1995.

[Kuz17] S. P. Kuznetsov. Regular and chaotic motions of the Chaplygin sleigh with periodically switched location of nonholonomic constraint. *Europhysics Letters*, 118(1):10007, 2017.

[Kuz18] S. P. Kuznetsov. Regular and chaotic dynamics of a Chaplygin Sleigh due to periodic switch of the nonholonomic constraint. *Regular and Chaotic Dynamics*, 23(2):178-192, 2018.

[LS04] J. S. W. Lamb, O. V. Stenkin. Newhouse regions for reversible systems with infinitely many stable, unstable and elliptic periodic orbits. *Nonlinearity*, 17(4):1217–1244, 2004.

[LT12] L. M. Lerman, D. Turaev. Breakdown of symmetry in reversible systems. *Regular and Chaotic Dynamics*, 17(3-4):318–336, 2012.

[Mal44] I. G. Malkin. On the stability under uniformly influencing perturbations. *Prikl. matem. i mech*, 8(3):241-245, 1944.

[QR92] J. A. G. Roberts, G. R. W. Quispel. Chaos and time-reversal symmetry. Order and chaos in reversible dynamical systems. *Physics Reports*, 216(2-3):63–177, 1992.

[Rue81] D. Ruelle. Small random perturbations of dynamical systems and the definition of attractors. *Communications in Mathematical Physics*, 82(1):137-151, 1981.

[Sev86] M. B. Sevryuk, Reversible systems. *Springer*, v. 1211, 2006.

[SSK17] E. A. Samylina, A. I. Shyhmamedov, A. O. Kazakov. On the structure of resonances under reversible perturbations of conservative cubic Henon maps. *Dinamicheskie Sistemy*, 7/35(3):229–244, 2017.

[SV09] C. Simó, A. Vieiro. Resonant zones, inner and outer splitting in generic and low order resonances of area preserving maps. *Nonlinearity*, 22(5):1191–1245, 2009.

[Tur10] D. Turaev. Richness of chaos in the absolute Newhouse domain. *Proceedings of the International Congress of Mathematicians 2010 (ICM 2010)* (In 4 Volumes) Vol. I: Plenary Lectures and Ceremonies Vols. II-IV: Invited Lectures, pp. 1804-1815, 2010.

[Tur15] D. Turaev. Maps close to identity and universal maps in the Newhouse domain. *Comm. Math. Phys.*, 335:1235-1277, 2015.